Modeling and Simulation of the Crystallization Behavior of Polymer Melts in the Hollow-Profile Extrusion Process Using the Coexistence Model of Spherulite and Shish-Kebab

Yue Mu,* Guoqun Zhao,* Anbiao Chen, Xianghong Wu

The thermally and flow induced crystallization behavior of polymer melts has been investigated by using penalty finite element-finite difference simulation with a decoupled solving algorithm. The coexistence model of spherulite and shish-kebab is proposed to describe the evolution of crystallization kinetics process. The Schneider equation and Eder equation are adopted to discriminate the relative roles of the thermal and the flow effect on the crystallization behavior. The proposed mathematical model and numerical method have been successfully applied to the investigation of crystallization behavior in the hollow-profile extrusion process. Both the evolution of crystalline size within the extrusion die and the effects of processing conditions on the crystallization kinetics process are discussed.

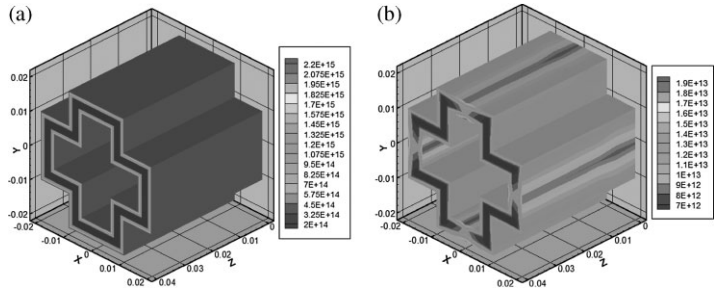

1. Introduction

The final properties of polymer products are to a great extent determined by the internal structure that developed during practical processing like extrusion, injection molding, and blow molding. Both the flow and thermo-mechanical history experienced within the die/mold in practical processing can enhance the nucleation and growth of crystallite, accelerate the crystallization kinetics process and lead to different types of crystalline structure. However, traditionally theoretical and experimental research methods are still difficult to afford to solve this strongly nonlinear problem. Numerical simulation as a highly effective method can successfully predict such complex phenomenon as in polymer processing and hence to explain relevant mechanism. Accurate prediction of material forming mechanism in practical processing by computer simulation requires not only appropriate mathematical model that considering the characteristics of crystallization behavior of polymer melts but also robust numerical solution method for solving the complicated nonlinear mathematical model.

From last several years, many researchers have dedicated to investigate and explain the mechanism of crystallization behavior in polymer processing. Doufas[1]

Y. Mu, G. Zhao, X. Wu
Key Laboratory for Liquid-Solid Structural Evolution and Processing of Materials, Ministry of Education, Shandong University, Jinan, Shandong 250061, China
E-mail: zhaogq@sdu.edu.cn, ymu@sdu.edu.cn
Y. Mu, G. Zhao, A. Chen, X. Wu
Engineering Research Center for Mold and Die Technologies, Shandong University, Jinan, Shandong 250061, China
Y. Mu
Key Laboratory of Materials Processing and Die and Mold Technology, Huazhong University of Science and Technology, Wuhan, Hubei 430074, China

DOI: 10.1002/mats.201200028

deduced a constitutive equation for the flow induced crystallization behaviors of polymer melts in uniform flow field based on Hamiltonian/Poisson theory. The micro-rheological model that can depict the microscopic morphology of polymer melts was adopted in Coppola's work[2] to establish the flow induced crystallization model, where the variation of conformational structure caused by the flow field should change the system free energy. Tanner and Qi[3] proposed a suspension model for polymer solidification at low shear rate. The spherulites were seemed as hard spheres that suspended in the amorphous phase and the stress distribution was calculated based on the hypothesis of concentrated suspension system. Zuidema et al.[4] considered the recovery strain as the driving force of flow induced crystallization by using the Leonov constitutive model. Zheng and Kennedy[5] presented an idea that to insert the free energy term calculated with the conformation tensor model into the Eder nucleation rate equation[6] to predict the flow induced crystallization behavior of poly(propylene). Yu et al.[7] developed a modified two-phase microstructure rheological model that can predict the evolution of viscosity and modulus under the flow state to investigate the flow induced crystallization behavior of the supercooling polymer melts. Most of recent researches are still aiming at solving supposed or simplified numerical examples including the hypothesis of material parameters and flow domain characteristics. It can be acceptable for the establishment of theoretical model or training of the numerical algorithm. However, from an industrial viewpoint, a more rigorous model and solving approach for practical polymer processing is necessary to capture the characteristics of crystallization behavior and reveal corresponding mechanism.

Although many theories have been proposed to model the crystallization kinetics process of polymeric material, the difficulty in solving the complicated governing equations for the thermally and flow induced crystallization behavior hinders the application of the proposed theoretical model to practical polymer processing. In the present study, the crystallization behavior of polymer melts within the hollow profile extrusion die is investigated by using finite element-finite difference simulation. The three-dimensional mathematical model of viscoelastic flow of polymer melts is established with a differential Phan-Thien and Tanner (PTT) constitutive model. The Schneider's approach and the Eder's model are employed to discriminate the relative roles of the thermal and the flow effect on the crystallization behavior. The coexistence model of spherulite and shish-kebabs is proposed to describe and quantify the evolution of thermally and flow induced crystalline structure. The corresponding finite element-finite difference model is derived and the details of numerical schemes are introduced. The penalty finite element method and a decoupled solving method are adopted to reduce computational memory requirement. The computation stability is improved by using the discrete elastic viscous split stress algorithm incorporating the streamline upwind scheme. The ellipticity of the momentum equation is improved by the addition of a stabilization factor. The influence of convective term in the constitutive equation and the energy equation is controlled by using asymmetric weighting function. The theoretical model and numerical method proposed in the study can not only describe the variation of macroscopic rheological parameters but also provide information on the variation of crystallizing morphology. The thermally and flow induced crystallization characteristics of polymer melts in the hollow profile extrusion process are investigated based on the established mathematical model and numerical algorithm. Both the distribution of crystallites and the evolution of crystalline size within the extrusion die are obtained by using the finite element-finite difference simulation. The effects of processing conditions including the volume flow rate and the die wall temperature on the crystallization kinetics process are further discussed.

2. Mathematical Modeling

2.1. Balance Equations

According to the theory of rheology, the governing equations to solve the crystallization problem of polymer melts can be obtained from the continuity equation (Equation 1), momentum equation (Equation 2), and energy equation (Equation 3), respectively, based on the conservation of mass, momentum, and energy.

$$\nabla\cdot\boldsymbol{u} = 0 \tag{1}$$

$$\rho\left(\frac{\partial \boldsymbol{u}}{\partial t} + \boldsymbol{u}\cdot\nabla\boldsymbol{u}\right) = \nabla\cdot\tau - \nabla p \tag{2}$$

$$\rho C_{\mathrm{p}}\left(\frac{\partial T}{\partial t} + \boldsymbol{u}\cdot\nabla T\right) = k\nabla\cdot(\nabla T) + \tau : \nabla\boldsymbol{u} + \rho\alpha_{\infty}\Delta H_{\mathrm{c}}\frac{\partial \alpha}{\partial t} \tag{3}$$

where ρ is the material density, $\boldsymbol{u}$ is the flow velocity, $\bigtriangledown$ is the Hamilton differential operator, t means time, $\boldsymbol{\tau}$ is the extra stress tensor, p is the hydrostatic pressure, C_{p} is the specific heat, T is the temperature, k is the thermal conductivity, α_{∞} is the absolute crystallinity, ΔH_{c} is the latent heat of crystallization, and α is the relative crystallinity.

A general Maxwell-type differential constitutive equation is adopted to model the viscoelastic properties of polymer melts. The rheological properties of the polymer solutions are here represented as the sum of a Newtonian solvent contribution with a PTT polymer contribution as follows

$$\tau = 2\eta_{\mathrm{v}}\boldsymbol{d} + \boldsymbol{S} \tag{4}$$

where η_v is the Newtonian-contribution viscosity, $\boldsymbol{d}=(\bigtriangledown\boldsymbol{u}+\bigtriangledown\boldsymbol{u}^{\mathrm{T}})/2$ is the deformation rate tensor and $\boldsymbol{S}$ is the polymer-contribution stress that obeys the equation

$$\lambda\overset{\square}{\boldsymbol{S}}+g(\boldsymbol{S})\,\boldsymbol{S}=2\eta_p\boldsymbol{d} \tag{5}$$

where λ is the relaxation time, η_p is the polymer-contribution viscosity and $g(\boldsymbol{S})$ is a stress function following the exponential form proposed in the original work of Phan-Thien and Tanner[8]

$$g(\boldsymbol{S})=\exp\left(\frac{\lambda\varepsilon}{\eta_p}tr(\boldsymbol{S})\right) \tag{6}$$

The full PTT constitutive model based on Gordon-Schowalter (GS) convective derivative is adopted and $\overset{\square}{\boldsymbol{S}}$ denotes the following Gordon-Schowalter convective derivative operator

$$\overset{\square}{\boldsymbol{S}}=\frac{\partial\boldsymbol{S}}{\partial t}+\boldsymbol{u}\cdot\nabla\boldsymbol{S}-(\nabla\boldsymbol{u}-\xi\boldsymbol{d})\cdot\boldsymbol{S}-\boldsymbol{S}\cdot(\nabla\boldsymbol{u}-\xi\boldsymbol{d})^{T} \tag{7}$$

Equation 7 can be simplified into the upper convective derivative when the parameter ξ of the GS derivative is set to zero.

2.2. Crystallization Kinetics Model

The crystallization of polymer melts can be described as the nucleation and growth process of crystallites. The nuclei are activated and grow into crystallites at rates depending on the flow and the thermomechanical state of the molten polymers in processing. In order to discriminate the thermal effect and the flow effect on the crystallization kinetic process in polymer processing, two kinds of crystallites that induced by the thermal state and the flow state are described by using the spherulite model and the shish-kebab model, respectively. The evolution of crystalline structure in practical polymer processing can then be more realistically quantified with the coexistence model of spherulite and shish-kebab.

The Schneider equations are adopted in the study to model the thermally induced crystallization process by means of a set of first order differential equations that describing the concepts of nucleation rate $\dot{N}(t)$ and spherulitic growth rate $G(t)$[9,10] as follows

$$\begin{cases}\dfrac{\partial\varphi_3^T(t)}{\partial t}+\boldsymbol{u}\cdot\nabla\varphi_3^T(t)=8\pi\dot{N}^T(t)\\ \dfrac{\partial\varphi_2^T(t)}{\partial t}+\boldsymbol{u}\cdot\nabla\varphi_2^T(t)=G(t)\varphi_3^T(t)\\ \dfrac{\partial\varphi_1^T(t)}{\partial t}+\boldsymbol{u}\cdot\nabla\varphi_1^T(t)=G(t)\varphi_2^T(t)\\ \dfrac{\partial\varphi_0^T(t)}{\partial t}+\boldsymbol{u}\cdot\nabla\varphi_0^T(t)=G(t)\varphi_1^T(t)\end{cases} \tag{8}$$

where φ_0^T is the total extended volume of the spherulite per unit volume if impingement is disregarded, φ_1^T is the total surface area of the spherulite per unit volume, φ_2^T is proportional to the sum of the spherulite radii per unit volume, φ_3^T is proportional to the number of the spherulites per unit volume.

Simultaneous with the spherulitic nucleation and growth process, the flow induced crystallization takes place in polymer processing. The crystalline structure like shish-kebab can be formed due to the influence of flow and deformation.[11,12] In the study, the Eder's rate equations are adopted to describe this contribution and the flow induced crystalline structure is represented by using cylindrical volume as follows

$$\begin{cases}\dfrac{\partial\varphi_3^f(t)}{\partial t}+\boldsymbol{u}\cdot\nabla\varphi_3^f(t)+\dfrac{\varphi_3^f(t)}{\lambda_n}=8\pi\left(\dfrac{\dot{\gamma}}{\dot{\gamma}_n}\right)^2 g_n\\ \dfrac{\partial\varphi_2^f(t)}{\partial t}+\boldsymbol{u}\cdot\nabla\varphi_2^f(t)+\dfrac{\varphi_2^f(t)}{\lambda_l}=\varphi_3^f(t)\left(\dfrac{\dot{\gamma}}{\dot{\gamma}_l}\right)^2 g_l\\ \dfrac{\partial\varphi_1^f(t)}{\partial t}+\boldsymbol{u}\cdot\nabla\varphi_1^f(t)=G(t)\varphi_2^f(t)\\ \dfrac{\partial\varphi_0^f(t)}{\partial t}+\boldsymbol{u}\cdot\nabla\varphi_0^f(t)=G(t)\varphi_1^f(t)\end{cases} \tag{9}$$

where $\dot{\gamma}$ is the shear rate, λ_n is the relation time for the nuclei formation, $\dot{\gamma}_n$ is a typical value for the shear rate for the nuclei growth, g_n is a parameter for the nucleation rate, λ_l is the relation time for the shish during axial growth, $\dot{\gamma}_l$ is a typical value for the shear rate for the extension of the shish, g_l is a parameter for the axial shish growth, φ_0^f is the total extended volume of the shish-kebab per unit volume if impingement is disregarded, φ_1^f is the total surface area of the shish-kebab per unit volume, φ_2^f is proportional to the total length of the shish per unit volume, φ_3^f is proportional to the number of the flow induced nuclei per unit volume.

The correction for the impingements is then introduced by using the Avrami equation and the following relative crystallinity can be derived

$$\alpha(t)=1-\exp(-\varphi_0^g(t)) \tag{10}$$

where $\varphi_0^g(t)=\varphi_0^T(t)+\varphi_0^f(t)$ is the extended global crystalline volume fraction obtained by adding the thermally induced extended crystalline volume and the flow induced extended crystalline volume.

The thermally induced nuclei number N^T in the molten polymer melts depends on the degree of supercooling ΔT as follows

$$N^T(t)=\exp(a\Delta T(t)+b) \tag{11}$$

where $\Delta T(t) = T_m - T(t)$, T_m is the equilibrium melting temperature, a and b are two material parameters to be identified with experiments.

The growth rate of the nuclei $G(t)$ is considered to be depended on the thermal state and the following Hoffman-Lauritzen expression is adopted

$$G(t) = G_0 \exp\left(-\frac{U^*}{R(T(t) - T_\infty)}\right)\exp\left(-\frac{K_g}{T(t)\Delta T}\right) \quad (12)$$

where U^* is the activation energy, R is the gas constant, $T_\infty = T_g - 30\,^\circ\mathrm{C}$ is the temperature below which molecular motion becomes impossible, T_g is the glass transition temperature, parameters G_0, and K_g can be determined by experiment.

3. Numerical Algorithm

3.1. Solution Method

As for the numerical simulation of thermally and flow induced crystallization of polymer melts, the efficiency in terms of memory requirement and time consumption, as well as the precision and stability of the numerical schemes are critical issues that should be well considered in the numerical modeling work. In the study, the penalty function method is employed to solve the nonlinear system consisting of the continuity equation and the momentum equation.[13] The penalty factor as a function obeying $\lambda_p = -(p/(\nabla\cdot\boldsymbol{u}))$ is firstly introduced to avoid a direct calculation of the hydrostatic pressure and hence to reduce the computation memory requirement. The following momentum governing equation can be obtained

$$\rho\left(\frac{\partial \boldsymbol{u}}{\partial t} + \boldsymbol{u}\cdot\nabla\boldsymbol{u}\right) - \nabla(\lambda_p\nabla\cdot\boldsymbol{u}) - 2\eta_v\nabla\cdot\boldsymbol{d} - \nabla\cdot\boldsymbol{S} = 0 \quad (13)$$

To improve the convergence property of the numerical scheme, the discrete elastic viscous split stress formulation is adopted and an ellipticity factor $2\overline{\eta}[\Sigma(\boldsymbol{u}) - \boldsymbol{d}]$ is introduced into the momentum equation (Equation 17).[14] The following equation is thus obtained

$$\rho\left(\frac{\partial \boldsymbol{u}}{\partial t} + \boldsymbol{u}\cdot\nabla\boldsymbol{u}\right) - \lambda_p\nabla(\nabla\cdot\boldsymbol{u}) + 2\overline{\eta}\nabla\cdot\Sigma(\boldsymbol{u}) = \nabla\cdot\boldsymbol{S} + 2(\overline{\eta} + \eta_v)\nabla\cdot\boldsymbol{d} \quad (14)$$

where $\Sigma(\boldsymbol{u}) = (\nabla\boldsymbol{u} + \nabla^T\boldsymbol{u})/2$, $\overline{\eta}$ is a reference viscosity.

The nonlinear system comprised by the flow balance equations and the crystallization kinetics equations can be used to predict the thermally and flow induced crystallization behavior of polymer melts in practical processing. The governing equations are numerically discretized in the time and the spatial domain, respectively, by using the finite differential method and the finite element method. The simulation flow chart of the thermally and flow induced crystallization can be seen from Figure 1.

A decoupled iteration method is employed to solve the governing equations including continuity equation, momentum equation, energy equation, constitutive equation, Schneider equation, and Eder equation in current time step. The velocity vector is firstly solved from Equation 15 by treating the polymer-contribution stress tensor and the deformation rate tensor as known terms

$$\rho\left(\frac{\partial \boldsymbol{u}^i}{\partial t} + \boldsymbol{u}^i\cdot\nabla\boldsymbol{u}^i\right) - \lambda_p\nabla(\nabla\cdot\boldsymbol{u}^i) + 2\overline{\eta}\nabla\cdot\Sigma(\boldsymbol{u}^i) = \nabla\cdot\boldsymbol{S}^{i-1} + 2(\overline{\eta} + (1-\beta)\eta_t)\nabla\cdot\boldsymbol{d}^{i-1} \quad (15)$$

where $\boldsymbol{d}^{i-1}$ and $\boldsymbol{S}^{i-1}$ are, respectively, the deformation rate tensor and the stress tensor calculated within the flow field at previous iteration step $i-1$ and their initial values are derived from viscous flow field, i is the current iteration step of flow field calculation.

The polymer-contribution stress tensor is then calculated through the constitutive equation (Equation 16) based on the velocity solution obtained from the calculation of the momentum equation (Equation 15).

$$\lambda\left(\frac{\partial \boldsymbol{S}^i}{\partial t} + \boldsymbol{u}^i\cdot\nabla\boldsymbol{S}^i - (\nabla\boldsymbol{u}^i)\cdot\boldsymbol{S}^i - \boldsymbol{S}^i\cdot(\nabla\boldsymbol{u}^i)^T + \frac{\xi}{2}\left((\nabla\boldsymbol{u}^i + (\nabla\boldsymbol{u}^i)^T)\cdot\boldsymbol{S}^i + \boldsymbol{S}^i\cdot(\nabla\boldsymbol{u}^i + (\nabla\boldsymbol{u}^i)^T)\right)\right) + \left(\exp\left(\frac{\lambda\varepsilon}{\eta_p}tr(\boldsymbol{S}^{i-1})\right)\right)\boldsymbol{S}^i = \eta_p\left(\nabla\boldsymbol{u}^i + (\nabla\boldsymbol{u}^i)^T\right) \quad (16)$$

where the nonlinear term $\exp\left((\lambda\varepsilon/\eta_p)tr(\boldsymbol{S}^{i-1})\right)$ is derived from the stress tensor obtained from last iteration step $i-1$.

Based on the velocity vector and stress tensor, respectively, obtained from Equation 15 and 16, the temperature field is then calculated from the energy equation

$$\rho C_p\left(\frac{\partial T^i}{\partial t} + \boldsymbol{u}^i\cdot\nabla T^i\right) = k\nabla\cdot(\nabla T^i) + \tau^i : \nabla\boldsymbol{u}^i + \rho\alpha_\infty\Delta H_c\frac{\partial\alpha^{i-1}}{\partial t} \quad (17)$$

where the terms on the right hand side, respectively, correspond to the heat exchange, the viscous heat

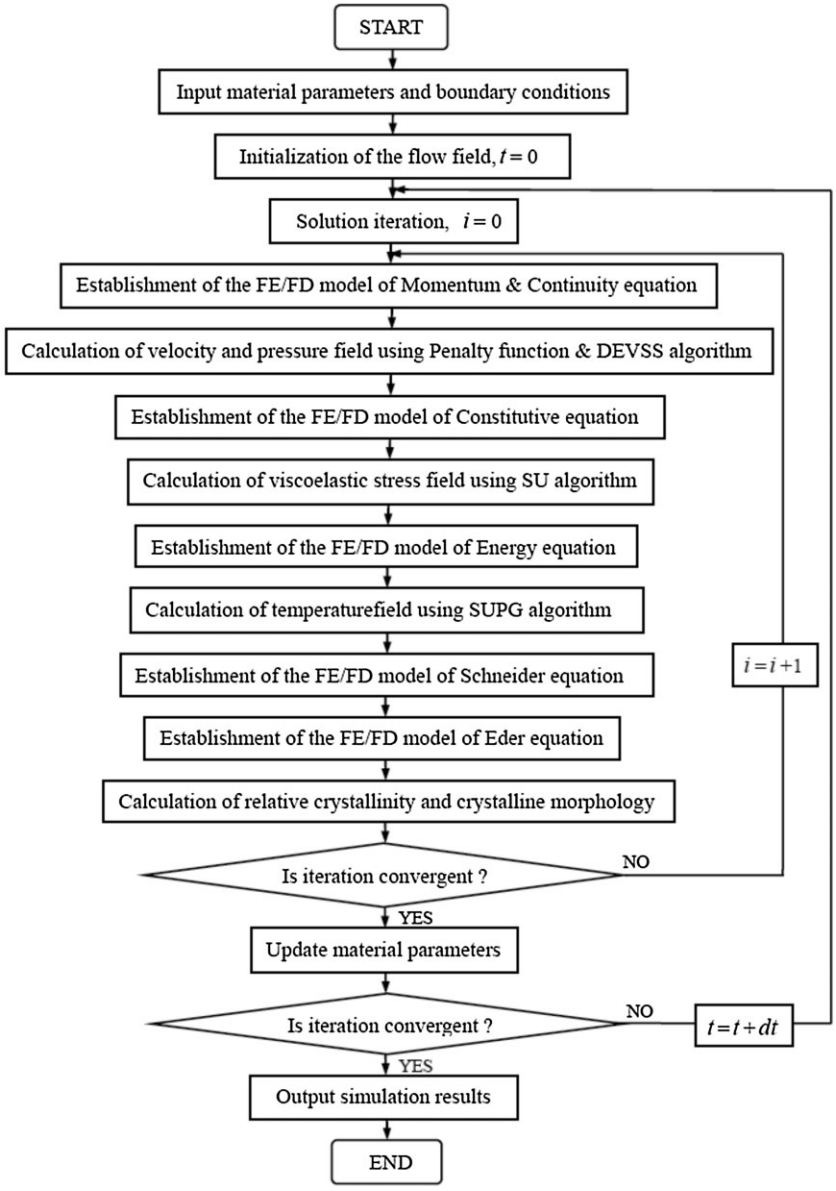

Figure 1. Simulation flow chart of the thermally and flow induced crystallization.

dissipation and the release of latent heat due to crystallization.

According to the calculation results of the flow and temperature field, the number of thermally induced nuclei and the growth rate of crystallites can be obtained. Both the relative crystallinity and the information on crystalline structure can then be solved based on the thermally and flow induced crystallization kinetics model as depicted in Section 2.2.

The convergence criteria of calculation within the current flow field are defined upon the following requirements as in Equation 18. When the average relative error of each variable is less than a set value, calculation convergence is considered to be achieved.

$$\begin{aligned} &\frac{1}{n}\sum\left|\frac{u^i - u^{i-1}}{u^i}\right| < \delta_u, \quad \frac{1}{n}\sum\left|\frac{S^i - S^{i-1}}{S^i}\right| < \delta_S, \\ &\frac{1}{n}\sum\left|\frac{T^i - T^{i-1}}{T^i}\right| < \delta_T, \quad \frac{1}{n}\sum\left|\frac{\alpha^i - \alpha^{i-1}}{\alpha^i}\right| < \delta_\alpha \end{aligned} \tag{18}$$

where n is the total number of finite element nodes in the computational domain, δ_u is the convergence criteria of the velocity vector which is set to 10^{-4}, δ_S is the convergence criteria of the polymer-contribution stress tensor which is set to 10^{-3}, δ_T is the convergence criteria

of the temperature which is set to 10^{-4}, and δ_α is the convergence criteria of the relative crystallinity which is set to 10^{-4} in the current study.

3.2. Finite Element Formulations

The Galerkin weighting residual method is adopted for the discretization of the momentum equation where the weighting function is taken as the same form as the interpretation function. After Green-Gauss transformation, the following weak form of Equation 14 can be obtained,

$$\begin{aligned}&\int_{\Omega^e} \boldsymbol{N}\left(\rho\left(\frac{\partial \boldsymbol{u}}{\partial t}+\boldsymbol{u}\cdot\nabla\boldsymbol{u}\right)\right)\mathrm{d}\Omega+\int_{\Omega^e}\nabla\boldsymbol{N}(\overline{\eta}(\nabla\boldsymbol{u}+\nabla\boldsymbol{u}^T)\\&-\lambda_{\mathrm{p}}(\nabla\cdot\boldsymbol{u}))\,\mathrm{d}\Omega=\int_{\Omega^e}\nabla\boldsymbol{N}(\boldsymbol{S}+2(\overline{\eta}+\eta_{\mathrm{v}})\boldsymbol{d})\\&+\int_{S^e}\boldsymbol{N}^*(\boldsymbol{S}-p\boldsymbol{I})\cdot\boldsymbol{n}\mathrm{d}S\end{aligned}\tag{19}$$

where $\boldsymbol{N}^*$ is equal to the interpolation function on the boundary force, Ω^e and S^e are, respectively, the element region and element boundary, and $\boldsymbol{n}$ is the outer normal unit vector.

The discretized momentum Equation 19 is then expanded along three directions of coordinate components (x, y, z) and the following elemental stiffness matrix equation can be obtained.

$$\begin{bmatrix}\left[k_{xx}^{ij}\right] & \left[k_{xy}^{ij}\right] & \left[k_{xz}^{ij}\right]\\ \left[k_{yx}^{ij}\right] & \left[k_{yy}^{ij}\right] & \left[k_{yz}^{ij}\right]\\ \left[k_{zx}^{ij}\right] & \left[k_{zy}^{ij}\right] & \left[k_{zz}^{ij}\right]\end{bmatrix}\begin{Bmatrix}\left\{u_x^j\right\}\\ \left\{u_y^j\right\}\\ \left\{u_z^j\right\}\end{Bmatrix}+\begin{bmatrix}\left[n_{xx}^{ij}\right] & \left[n_{xy}^{ij}\right] & \left[n_{xz}^{ij}\right]\\ \left[n_{yx}^{ij}\right] & \left[n_{yy}^{ij}\right] & \left[n_{yz}^{ij}\right]\\ \left[n_{zx}^{ij}\right] & \left[n_{zy}^{ij}\right] & \left[n_{zz}^{ij}\right]\end{bmatrix}\begin{Bmatrix}\left\{\partial u_x^j/\partial t\right\}\\ \left\{\partial u_y^j/\partial t\right\}\\ \left\{\partial u_z^j/\partial t\right\}\end{Bmatrix}=\begin{Bmatrix}\left\{f_x^i\right\}\\ \left\{f_y^i\right\}\\ \left\{f_z^i\right\}\end{Bmatrix}\tag{20}$$

$$(i,j=1,2,\ldots,8)$$

According to the nodes superposition principle and element connectivity, the global stiffness matrix equation of the momentum Equation 21 for all the elements can be assembled after evaluating the elemental stiffness matrix at elemental level using Equation 20.

$$[K]\{\boldsymbol{u}\}_t+[N]\left\{\frac{\partial \boldsymbol{u}}{\partial t}\right\}_t=\{f\}_t\tag{21}$$

where $[K]$ is the global stiffness matrix of the unknown velocity vectors $\{\boldsymbol{u}\}$, $[N]$ is the transient diffusion matrix, $\{f\}$ corresponds to the equation residuals, and the subscript t denotes the current time step.

As for the discretization of constitutive equation, the effect of convective term $\boldsymbol{u}\cdot\nabla\boldsymbol{S}$ should be well considered. When the convective term becomes dominant as the Weissenberg number increases, the classical Galerkin weighting residual method will lose its optimal approximation. The inconsistent streamline upwind method is adopted here to control the convective effect and an asymmetric weighting function W is introduced,

$$\boldsymbol{W}=\boldsymbol{N}+\frac{\overline{k}\boldsymbol{u}}{(\boldsymbol{u}\cdot\boldsymbol{u})}\cdot\nabla\boldsymbol{N}\tag{22}$$

where $\boldsymbol{N}$ is equal to the classical Galerkin weighting function, the coefficient $\overline{k}$ is defined by the velocity components at the element center (u_ξ, u_η, u_ζ) as proposed by Marchal and Crochet[15]

$$\overline{k}=\frac{(u_\xi{}^2+u_\eta{}^2+u_\zeta{}^2)^{1/2}}{2}\tag{23}$$

The additional term of the weighting function $(\overline{k}\boldsymbol{u}/(\boldsymbol{u}\cdot\boldsymbol{u}))\cdot\nabla\boldsymbol{N}$ is only imposed on the purely advective term in the constitutive Equation 16 and the following elemental constitutive equation can be obtained

$$\begin{aligned}&\int_{\Omega^e}\boldsymbol{N}\left(\lambda\left(\frac{\partial\boldsymbol{S}}{\partial t}-(\nabla\boldsymbol{u}^i)\cdot\boldsymbol{S}-\boldsymbol{S}\cdot(\nabla\boldsymbol{u})^T\right.\right.\\&\left.\left.+\frac{\xi}{2}\left((\nabla\boldsymbol{u}+(\nabla\boldsymbol{u})^T)\cdot\boldsymbol{S}+\boldsymbol{S}\cdot(\nabla\boldsymbol{u}+(\nabla\boldsymbol{u})^T)\right)\right)\right)\mathrm{d}\Omega\\&+\int_{\Omega^e}\boldsymbol{W}(\lambda(\boldsymbol{u}\cdot\nabla\boldsymbol{S}))\,\mathrm{d}\Omega\\&+\int_{\Omega^e}\boldsymbol{N}\left(\left(\exp\left(\frac{\lambda\varepsilon}{\eta_{\mathrm{p}}}tr(\boldsymbol{S})\right)\right)\boldsymbol{S}\right)\mathrm{d}\Omega\\&=\int_{\Omega^e}\boldsymbol{N}\left(\eta_{\mathrm{p}}(\nabla\boldsymbol{u}+(\nabla\boldsymbol{u})^T)\right)\mathrm{d}\Omega\end{aligned}\tag{24}$$

Equation 24 is then expanded along three directions of coordinate components and the elemental stiffness matrix equation is obtained as follows

$$\begin{bmatrix} [k_{11}^{ij}] & [k_{12}^{ij}] & [k_{13}^{ij}] & 0 & 0 & 0 \\ [k_{21}^{ij}] & [k_{22}^{ij}] & [k_{23}^{ij}] & [k_{24}^{ij}] & [k_{25}^{ij}] & 0 \\ [k_{31}^{ij}] & [k_{32}^{ij}] & [k_{33}^{ij}] & 0 & [k_{35}^{ij}] & [k_{36}^{ij}] \\ 0 & [k_{42}^{ij}] & 0 & [k_{44}^{ij}] & [k_{45}^{ij}] & 0 \\ 0 & [k_{52}^{ij}] & [k_{53}^{ij}] & [k_{54}^{ij}] & [k_{55}^{ij}] & [k_{56}^{ij}] \\ 0 & 0 & [k_{63}^{ij}] & 0 & [k_{65}^{ij}] & [k_{66}^{ij}] \end{bmatrix} \begin{Bmatrix} \{S_{xx}^j\} \\ \{S_{xy}^j\} \\ \{S_{xz}^j\} \\ \{S_{yy}^j\} \\ \{S_{yz}^j\} \\ \{S_{zz}^j\} \end{Bmatrix} + \begin{bmatrix} [n_{11}^{ij}] & [n_{12}^{ij}] & [n_{13}^{ij}] & 0 & 0 & 0 \\ [n_{21}^{ij}] & [n_{22}^{ij}] & [n_{23}^{ij}] & [n_{24}^{ij}] & [n_{25}^{ij}] & 0 \\ [n_{31}^{ij}] & [n_{32}^{ij}] & [n_{33}^{ij}] & 0 & [n_{35}^{ij}] & [n_{36}^{ij}] \\ 0 & [n_{42}^{ij}] & 0 & [n_{44}^{ij}] & [n_{45}^{ij}] & 0 \\ 0 & [n_{52}^{ij}] & [n_{53}^{ij}] & [n_{54}^{ij}] & [n_{55}^{ij}] & [n_{56}^{ij}] \\ 0 & 0 & [n_{63}^{ij}] & 0 & [n_{65}^{ij}] & [n_{66}^{ij}] \end{bmatrix} \begin{Bmatrix} \{\partial S_{xx}^j/\partial t\} \\ \{\partial S_{xy}^j/\partial t\} \\ \{\partial S_{xz}^j/\partial t\} \\ \{\partial S_{yy}^j/\partial t\} \\ \{\partial S_{yz}^j/\partial t\} \\ \{\partial S_{zz}^j/\partial t\} \end{Bmatrix} = \begin{Bmatrix} \{f_1^i\} \\ \{f_2^i\} \\ \{f_3^i\} \\ \{f_4^i\} \\ \{f_5^i\} \\ \{f_6^i\} \end{Bmatrix} \quad (i,j = 1,2,\ldots,8) \tag{25}$$

The global stiffness matrix equation of the constitutive equation (Equation 26) for all the elements is assembled after the elemental calculation according to the nodes superposition principle.

$$[K]\{\boldsymbol{S}\}_t + [\boldsymbol{N}]\left\{\frac{\partial \boldsymbol{S}}{\partial t}\right\}_t = \{f\}_t \tag{26}$$

where $[K]$ is the global stiffness matrix of the unknown stress tensors $\{\boldsymbol{S}\}$, $[N]$ is the transient diffusion matrix, $\{f\}$ corresponds to the equation residuals, and the subscript t means the current time step.

The energy Equation 17 is a typical convection/diffusion problem and calculation oscillation probably occurs with the increase of the Peclet number Pe that defined as follows

$$Pe = \frac{\rho C_p \overline{u}}{k} \tag{27}$$

where $\overline{u}$ is the mean flow velocity in the downstream of the flow field.

The streamline upwind Petrov-Galerkin formulation is employed to control the undesirable oscillations in the calculation of temperature field. Another asymmetric weighting function $\boldsymbol{\Psi}$ is introduced in the study as follows

$$\boldsymbol{\Psi} = \boldsymbol{N} + \frac{\widetilde{k}\boldsymbol{u}}{\|\boldsymbol{u}\|^2}\cdot\nabla \boldsymbol{N} \tag{28}$$

where the coefficient $\widetilde{k} = (\widetilde{\xi}u_\xi h_\xi + \widetilde{\eta}u_\eta h_\eta + \widetilde{\zeta}u_\zeta h_\zeta)/2$ is related to the local Peclet number in each element as proposed by Brooks and Hughes.[16]

The weighting function $\boldsymbol{\Psi}$ is applied to all terms of the energy Equation 17 at the elemental level and the following elemental energy equation is obtained.

$$\begin{aligned} &\int_{\Omega^e} \Psi\left(\rho C_p\left(\frac{\partial T}{\partial t} + \boldsymbol{u}\cdot\nabla T\right)\right)\mathrm{d}\Omega = \int_{\Omega^e} \Psi(k\nabla^2 T)\mathrm{d}\Omega \\ &\quad + \int_{\Omega^e} \Psi\left(\boldsymbol{\tau} : \nabla \boldsymbol{u} + \rho\alpha_\infty \Delta H_c \frac{\partial \alpha}{\partial t}\right)\mathrm{d}\Omega \end{aligned} \tag{29}$$

After Green-Gauss transformation, the weak form of Equation 29 is obtained,

$$\begin{aligned} &\int_{\Omega^e} \Psi\left(\rho C_p\left(\frac{\partial T}{\partial t} + \boldsymbol{u}\cdot\nabla T\right)\right)\mathrm{d}\Omega + \int_{\Omega^e} \nabla\Psi(k\nabla T)\,\mathrm{d}\Omega \\ &= \int_{\Omega^e} \Psi\left(\boldsymbol{\tau} : \nabla \boldsymbol{u} + \rho\alpha_\infty \Delta H_c \frac{\partial \alpha}{\partial t}\right)\mathrm{d}\Omega + \int_{S^e} \Psi^*(k\nabla T)\cdot\boldsymbol{n}\mathrm{d}S \end{aligned} \tag{30}$$

where $\boldsymbol{\Psi}^*$ is equal to the interpolation function of the boundary force.

The discretized energy Equation 30 can be written as the following elemental stiffness matrix equation.

$$\begin{bmatrix} k_{11} & k_{12} & \dots & k_{18} \\ k_{21} & k_{22} & \dots & k_{28} \\ \vdots & \vdots & \ddots & \vdots \\ k_{81} & k_{82} & \dots & k_{88} \end{bmatrix} \begin{Bmatrix} T_1 \\ T_2 \\ \vdots \\ T_8 \end{Bmatrix} + \begin{bmatrix} n_{11} & n_{12} & \dots & n_{18} \\ n_{21} & n_{22} & \dots & n_{28} \\ \vdots & \vdots & \ddots & \vdots \\ n_{81} & n_{82} & \dots & n_{88} \end{bmatrix}$$

$$\begin{Bmatrix} \partial T_1/\partial t \\ \partial T_2/\partial t \\ \vdots \\ \partial T_8/\partial t \end{Bmatrix} = \begin{Bmatrix} f_1 \\ f_2 \\ \vdots \\ f_8 \end{Bmatrix} \tag{31}$$

According to the nodes superposition principle, the global stiffness matrix equation of the energy (Equation 32) for all the elements can be assembled after evaluating the elemental stiffness matrix at elemental level by using Equation 31,

$$[K]\{T\}_t + [N]\left\{\frac{\partial T}{\partial t}\right\}_t = \{f\}_t \tag{32}$$

where $[K]$ is the global stiffness matrix of the unknown variable $\{T\}$, $[N]$ is the transient diffusion matrix, $\{f\}$ corresponds to the equation residuals, and the subscript t means the current time step.

As for the Schneider Equation 8 and the Eder Equation 9, each differential equation can be written as the following convection diffusion equation

$$\frac{\partial \varphi}{\partial t} + \boldsymbol{u}\cdot\nabla\varphi = Q \tag{33}$$

According to classical Galerkin weighting residual method where the weighting function is taken as the same form as the interpretation function, the discretization form of the Schneider equation and the Eder equation can be obtained

$$\int_{\Omega^e} \boldsymbol{N}\left(\frac{\partial \varphi}{\partial t}\right) \mathrm{d}\Omega + \int_{\Omega^e} \boldsymbol{N}(\boldsymbol{u}\cdot\nabla\varphi)\,\mathrm{d}\Omega = \int_{\Omega^e} \boldsymbol{N}Q\,\mathrm{d}\Omega \tag{34}$$

The discretized Equation 34 can be written as the following elemental stiffness matrix equation,

$$\begin{bmatrix} k_{11} & k_{12} & \dots & k_{18} \\ k_{21} & k_{22} & \dots & k_{28} \\ \vdots & \vdots & \ddots & \vdots \\ k_{81} & k_{82} & \dots & k_{88} \end{bmatrix} \begin{Bmatrix} \varphi_1 \\ \varphi_2 \\ \vdots \\ \varphi_8 \end{Bmatrix} + \begin{bmatrix} n_{11} & n_{12} & & n_{18} \\ & n_{21} & n_{22} & \dots & n_{28} \\ \dots & \vdots & \vdots & \ddots & \vdots \\ & n_{81} & n_{82} & \dots & n_{88} \end{bmatrix}$$

$$\begin{Bmatrix} \partial\varphi_1/\partial t \\ \partial\varphi_2/\partial t \\ \vdots \\ \partial\varphi_3/\partial t \end{Bmatrix} = \begin{Bmatrix} f_1 \\ f_2 \\ \vdots \\ f_8 \end{Bmatrix} \tag{35}$$

The global stiffness matrix equation for all the elements is assembled after the elemental calculation according to the nodes superposition principle as follows

$$[K]\{\varphi\}_t + [N]\left\{\frac{\partial \varphi}{\partial t}\right\}_t = \{f\}_t \tag{36}$$

where $[K]$ is the global stiffness matrix of the unknown variable $\{\varphi\}$, $[N]$ is the transient diffusion matrix, $\{f\}$ corresponds to the equation residuals and the subscript t means the current time step.

3.3. Finite Element/Finite Difference Formulations

According to the definition of finite difference method, two-point difference scheme of a typical convection diffusion equation can be written as follows

$$a\left\{\frac{\partial C}{\partial t}\right\}_t + (1-a)\left\{\frac{\partial C}{\partial t}\right\}_{t-\Delta t} = \frac{1}{\Delta t}\left(\{C\}_t - \{C\}_{t-\Delta t}\right) \tag{37}$$

When different coefficient value a ($a = 1, 0, 1/2$ and $2/3$) is adopted in Equation 37, different difference schemes like the backward difference scheme, the forward difference scheme, the Crank-Nicolson difference scheme and the Galerkin difference scheme can be obtained. Among the above difference schemes, Crank-Nicolson difference scheme and Galerkin difference scheme are unconditionally stable and show higher calculation accuracy.

After discretized in the spatial domain by using finite element method, the basic governing equations of the thermally and flow induced crystallization model can

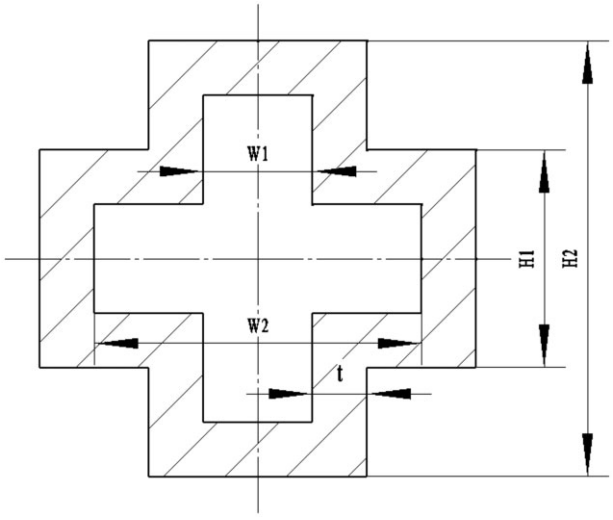

Figure 2. Section view of the hollow profile product.

all be written as the following format

$$[K]\{C\}_t + [N]\left\{\frac{\partial C}{\partial t}\right\}_t = \{f\}_t \tag{38}$$

where the variable $\{C\}$ can be used to denote the unknown variables like $\{\boldsymbol{u}\}$, $\{\boldsymbol{S}\}$, $\{T\}$, or $\{\varphi\}$.

The basic governing Equation 38 at the current time step t and the last time step $t - \Delta t$ can be, respectively, written as

$$\begin{cases} [K]\{C\}_t + [N]\left\{\dfrac{\partial C}{\partial t}\right\}_t = \{f\}_t \\ [K]\{C\}_{t-\Delta t} + [N]\left\{\dfrac{\partial C}{\partial t}\right\}_{t-\Delta t} = \{f\}_{t-\Delta t} \end{cases} \tag{39}$$

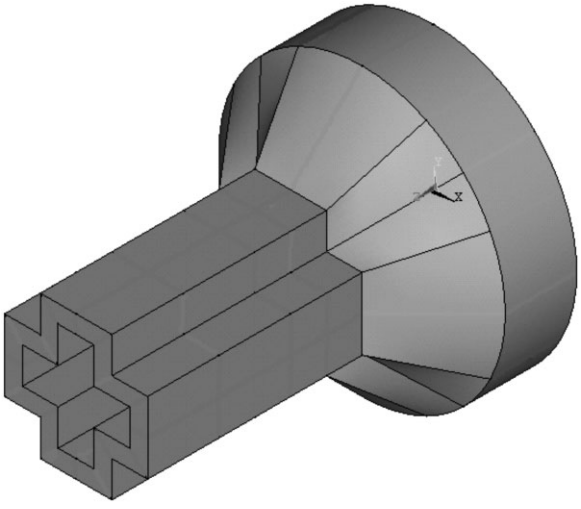

Figure 3. Geometrical model of the flow channel.

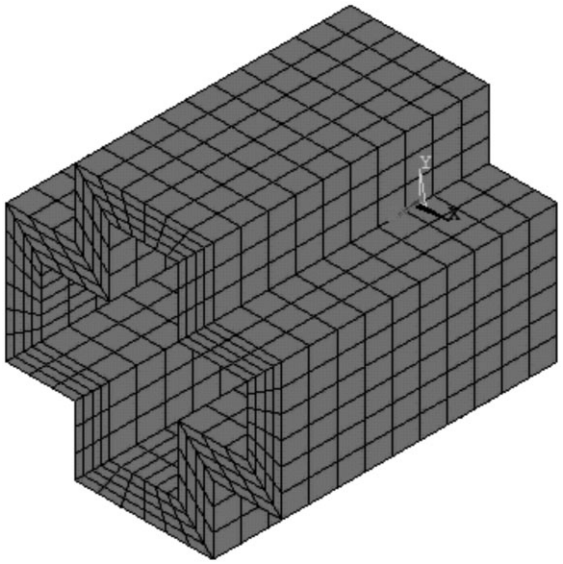

Figure 4. Finite element model of the crystallization region.

Substituting the Equation 39 into Equation 37, the following finite element-finite difference formulations with Crank-Nicolson difference scheme of the governing equations can thus be obtained

$$\left([K] + \frac{2[N]}{\Delta t}\right)\{C\}_t = (\{f\}_t + \{f\}_{t-\Delta t}) + \left(\frac{2[N]}{\Delta t} - [K]\right)\{C\}_{t-\Delta t} \tag{40}$$

Table 1. Physical properties of poly(propylene).

Parameter	Unit	Value
α_∞	–	0.7
ΔH_c	$J \cdot kg^{-1}$	5×10^4
a	K^{-1}	1.56×10^{-1}
b	–	1.51×10^1
T_m	°C	210
T_g	°C	−4
U^*	$J \cdot mol^{-1}$	6270
R	$J \cdot K^{-1} \cdot mol^{-1}$	8.31
K_g	K^2	5.5×10^5
G_0	$m \cdot s^{-1}$	2.83×10^2
λ, λ_n	s	4.0×10^{-2}
λ_1	s	∞
η_p	Pa · s	3411
$g_n/\dot{\gamma}_n^2$	–	4.685×10^{12}
$g_1/\dot{\gamma}_1^2$	–	2.69×10^{-10}

4. Application to the Extrusion Process

4.1. Modeling of the Hollow-Profile Extrusion Process

The thermally and flow induced crystallization behavior of poly(propylene) in the hollow profile extrusion process is investigated based on the mathematical model and numerical method proposed in the study. The section view of the profile is shown in Figure 2 where the inner width W_1 is 0.01 m, the outer width W_2 is 0.03 m, the inner height H_1 is 0.02 m, the outer height H_2 is 0.04 m, and the thickness t is 0.005 m. The geometric structure of the flow channel within the extrusion die is sketched in Figure 3, which consists of an adapter, transition region, parallel region, and cooling region. The crystallization of polymer melts mainly occurs in the cooling region as shown in Figure 4, and the solved domain is divided into tri-linear brick elements by means of mapping mesh generation technology which consists of 1920 elements and 2640 nodes. The physical properties of poly(propylene) detected by the dynamic rheometer, the differential scanning calorimeter and the shearing hot stage with polarizing microscope as listed in Table 1 are adopted in the numerical calculation.[17]

When the true boundary conditions are introduced into the governing equations, the corresponding calculation can reflect practical physical phenomenon. On the inflow boundary, the flow is fully developed and the axial velocity can be imposed with the radial velocity being set to zero. A fixed temperature boundary $T = T_{\text{inlet}}$ is also imposed on the inlet face. On the die wall, the non-slip condition can be imposed with all the velocity components being set to zero. Due to the vanishing of convective derivative in the constitutive equation, the stress components can be calculated iteratively in terms of the non-zero components

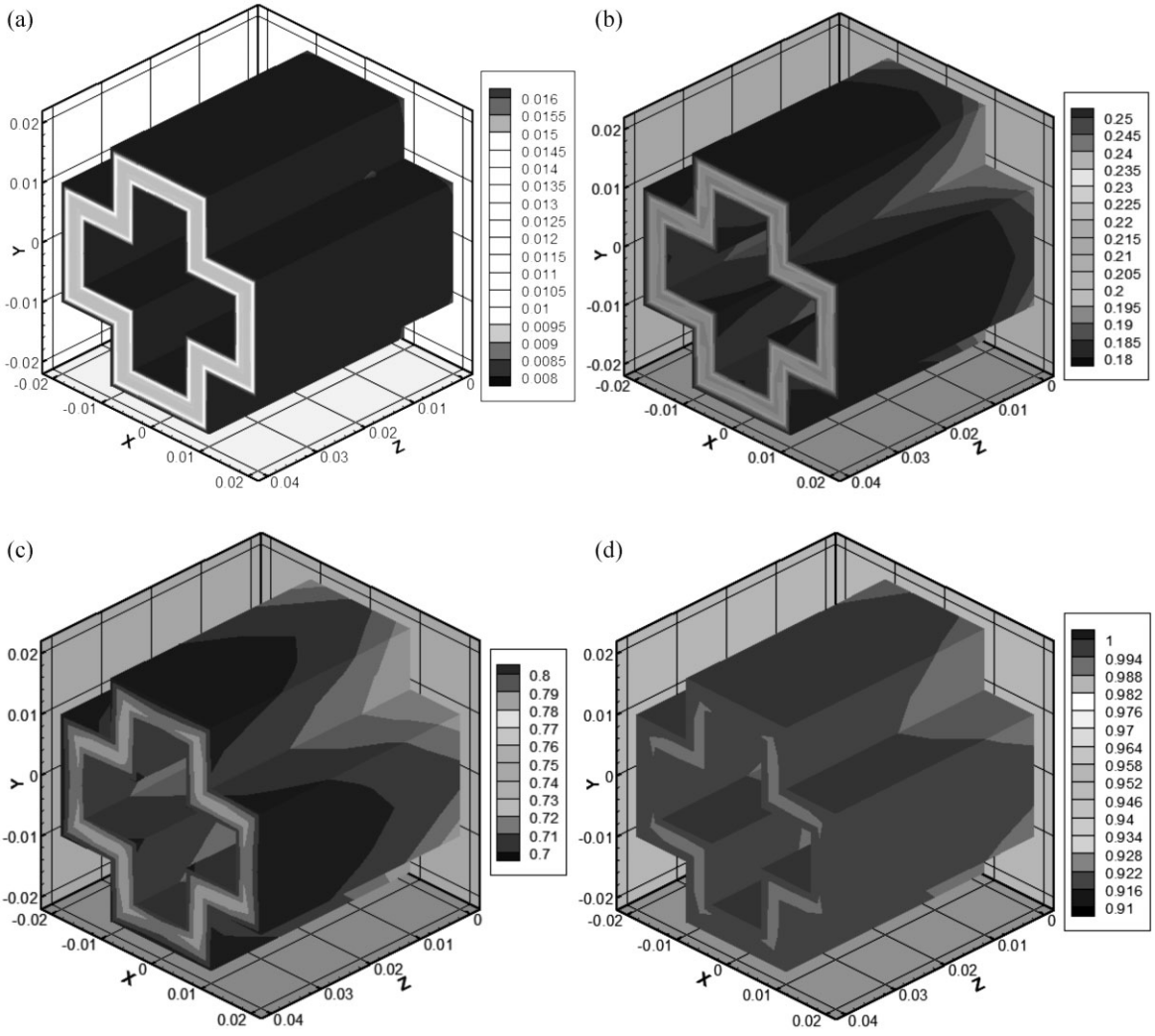

Figure 5. Variation of the relative crystallinity: $t =$ (a) 1 s, (b) 4 s, (c) 8 s, and (d) 12 s.

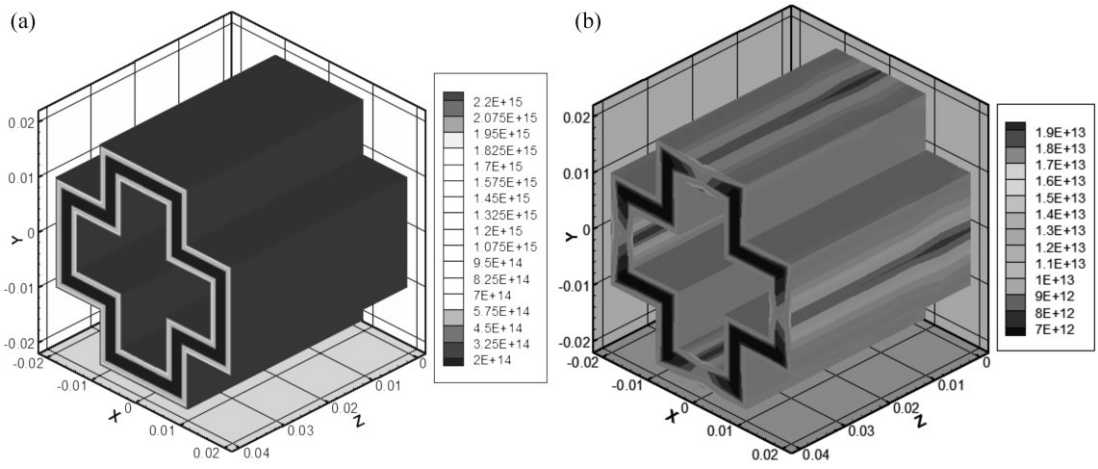

Figure 6. Distribution of the nucleation density at $t = 12$ s: (a) spherulite; (b) shish-kebab.

of the velocity gradients. An isothermal contact is imposed on the die wall and the melts temperature near the die wall is assigned to be $T = T_{wall}$. On the downstream outflow boundary, fully developed Neumann boundary conditions are set for all the variables except for the tangential velocity component that is supposed to vanish.

4.2. Crystallization Characteristics

4.2.1. Distribution of Crystallization Variables

According to practical processing conditions in the hollow profile extrusion, the inlet volume flow rate Q_v is set to be 1.4×10^{-5} m$^3 \cdot$ s^{-1}, the inlet temperature of polymer melts T_{inlet} is set to be 423 K and the temperature on the die wall T_{wall} is set to be 353 K. Based on the theoretical model and numerical algorithm proposed in the study, the crystallization characteristics of polymer melts within the hollow profile extrusion die are investigated as shown from

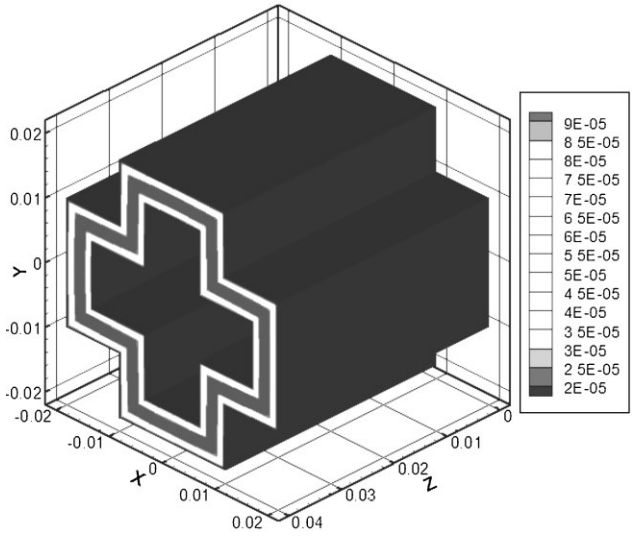

Figure 7. Distribution of the average crystallite radius of spherulite at $t = 12$ s (unit: m).

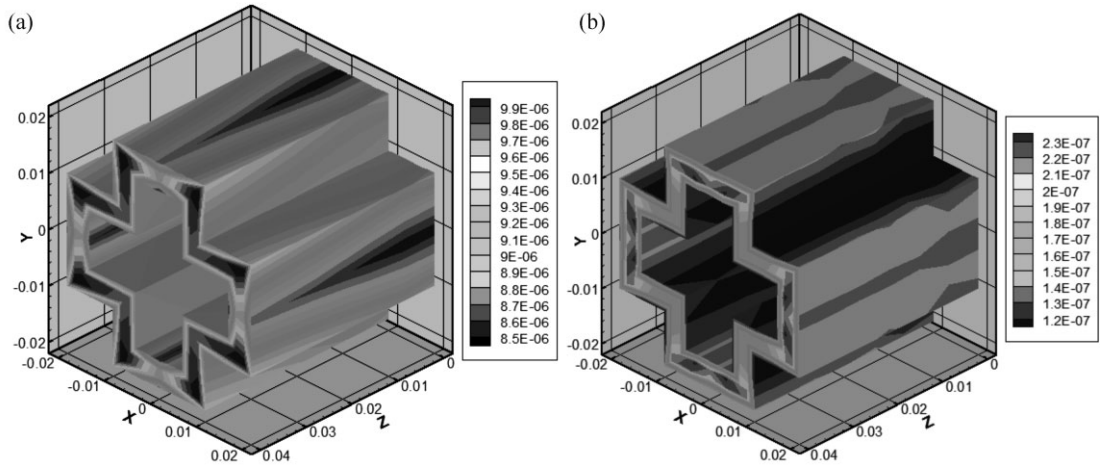

Figure 8. Distribution of the average crystallite size of shish-kebabs at $t = 12$ s (unit: m): (a) radius; (b) length.

Figure 5–8. Figure 5 shows the variation of relative crystallinity with the evolution of crystallization kinetics process. It can be found that the crystallization rate near the die wall is relatively larger than that within the flow channel. This is because both the supercooling degree and the shearing effect near the die wall are larger than those in the flow channel center, and hence accelerate the crystallization kinetics process. The relative crystallinity in the downstream of the flow channel is also found to be larger than that in the upstream of the flow channel, where polymeric material experiences longer shearing and cooling effects. Figure 6 shows the distribution of nucleation density of spherulite and shish-kebab, respectively, induced by the thermal and the flow state. It can be found that the nucleation density near the die wall is relatively larger than that within the flow channel for the reason of larger supercooling degree and stronger shearing effect. The thermally induced nucleation of spherulite is found to be dominated under the current processing conditions compared with the shish-kebab induced by shearing effect. Figure 7 and 8 show the distribution of the average crystallite size of the spherulite and the shish-kebab, respectively, induced by the thermal and the flow state. It can be found that the radius of spherulite near the die wall is smaller than that in the center of the flow channel for the reason of larger supercooling degree. Both the radius and the length of shish-kebab near the die wall is found to be smaller than those within the flow channel especially in the region where polymer melts experienced stronger shearing effect. That's the reason why a "skin/core" structure is usually found in practical polymer processing which influences the strength, toughness, permeability, surface texture, transparency, and other properties of final products.

4.2.2. Effects of the Processing Conditions

The volume flow rate and the thermal state are important processing parameters in the extrusion process that can influence the crystallization behavior of polymer melts, and hence affect the structure and property of the final products. The volume flow rate can be adjusted with the rotational speed of the extruder and the thermal state can be adjusted by the cooling system in the shaped mold. In the study, the effects of the processing conditions including the volume flow rate and the thermal state are investigated as shown from Figure 9–13. The variation of the nucleation density of the flow induced shish–kebab with different volume flow rates ($Q_v^1 = 7.0 \times 10^{-6}$ $m^3 \cdot s^{-1}$, $Q_v^2 = 1.4 \times 10^{-5}$ $m^3 \cdot s^{-1}$, $Q_v^3 = 2.8 \times 10^{-5}$ $m^3 \cdot s^{-1}$) at $t = 12$ s ($T_{wall} = 353$ K)is evaluated on the $z = 0.02$ cross-section as shown in Figure 9. It can be found that the nucleation density increases with the increase of the volume flow rate. The nucleation density near the die wall is larger than that within the flow channel, especially on the eight convex edges near the outer and inner die wall where stronger shearing occurs. Figure 10 shows the variation of the average crystallite size of the flow induced shish-kebab with different volume flow rates on the $z = 0.02$ cross-section at $t = 12$ s ($T_{wall} = 353$ K). It can

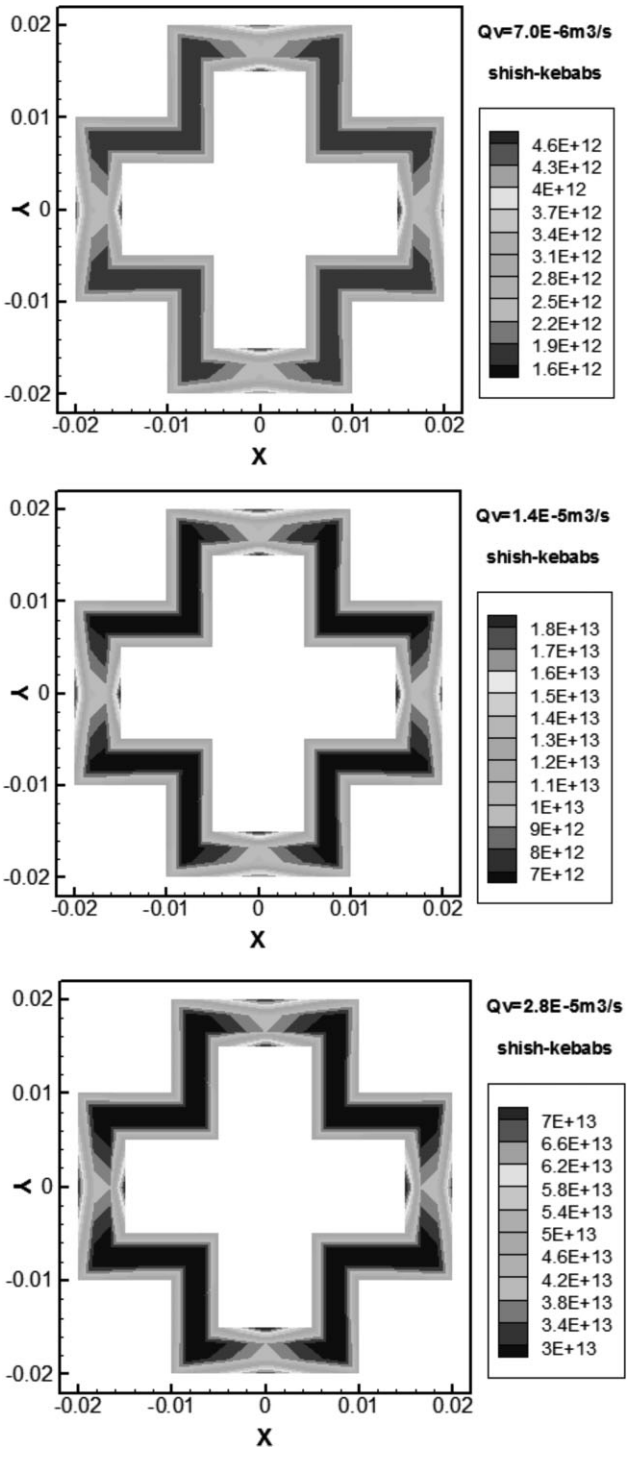

Figure 9. Variation of the nucleation density of shish-kebab, with different volume flow rates on the $z = 0.02$ cross-section at $t = 12$ s ($T_{wall} = 353$ K).

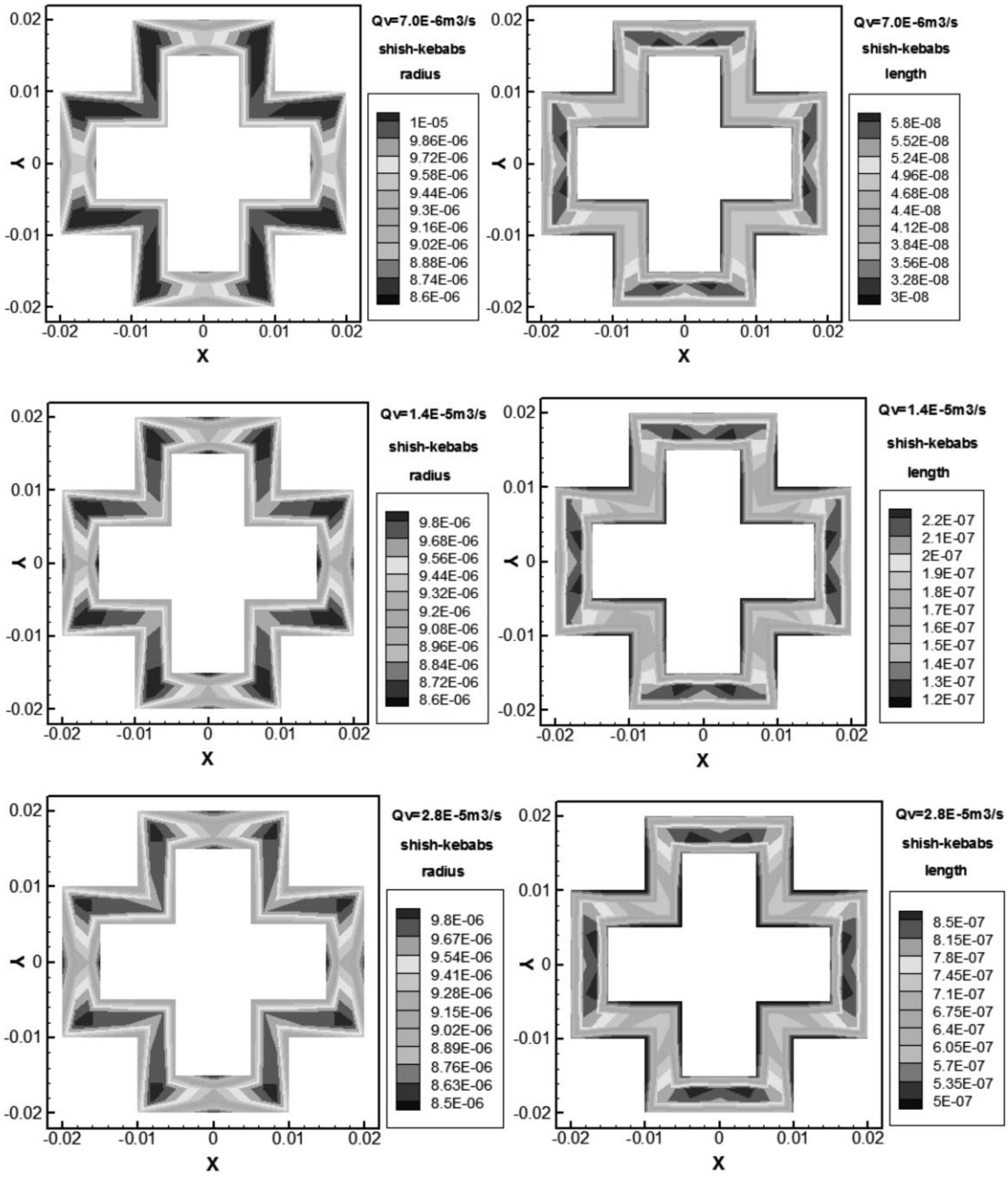

Figure 10. Variation of the average crystallite size of shish-kebab with different volume flow rates on the $z = 0.02$ cross-section at $t = 12$ s ($T_{wall} = 353$ K).

be found that the radius of the shish-kebab slightly changes with the variation of the volume flow rate. While in the mean while, the length of the shish-kebab increases with the increase of the volume flow rate. This is because the larger volume flow rate may result in stronger shearing effect that enhances the extension of the shish. The physical properties of final product along the orientation direction can hence be enhanced. The variation of the relative crystallinity with different thermal state ($T_{wall} = 333$ K, $T_{wall} = 353$ K, $T_{wall} = 373$ K)is evaluated on the $z = 0.02$ cross-section at $t = 5$ s ($Q_v = 1.4 \times 10^{-5}$ $m^3 \cdot s^{-1}$)as shown in Figure 11. It can be found that the crystallization rate is improved with the decrease of temperature on the die wall. This is because the supercooling degree of the polymer melts is increased with the decrease of the die wall temperature and hence to accelerate the crystal-

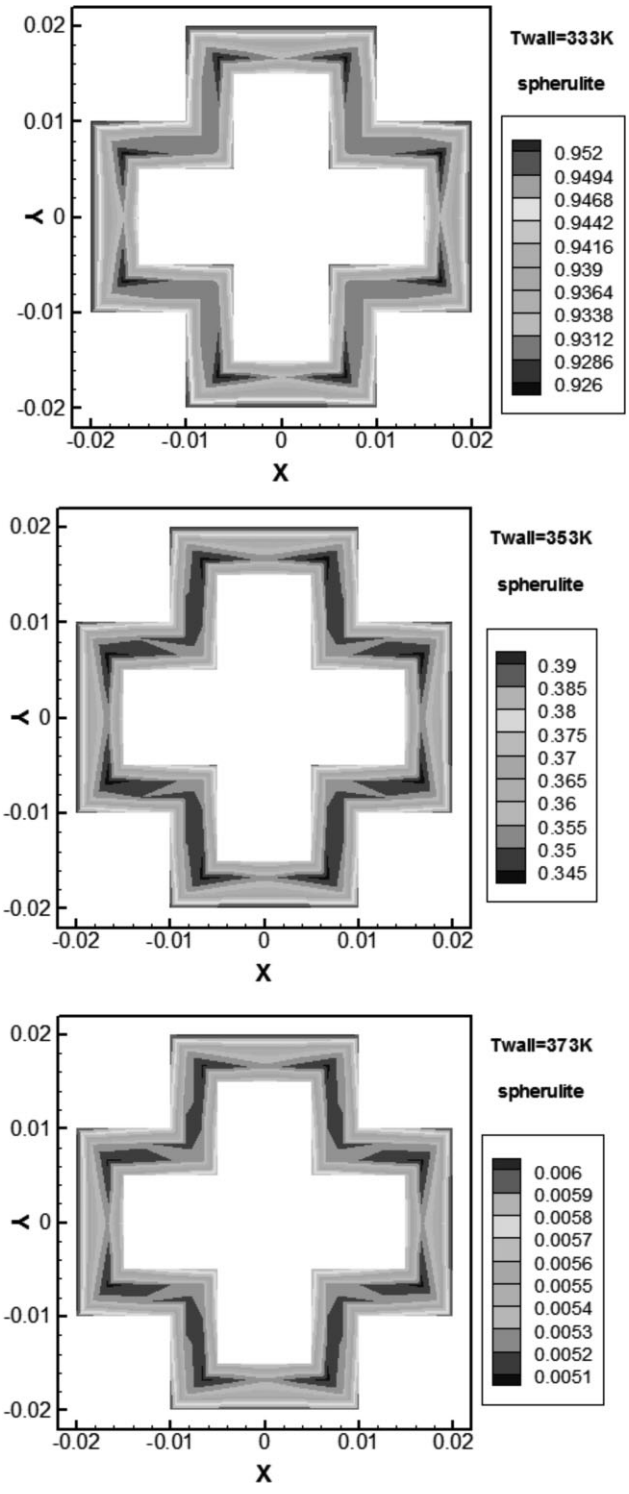

Figure 11. Variation of the relative crystallinity with different thermal state on the $z = 0.02$ cross-section at $t = 5$ s ($Q_v = 1.4 \times 10^{-5}\ m^3 \cdot s^{-1}$).

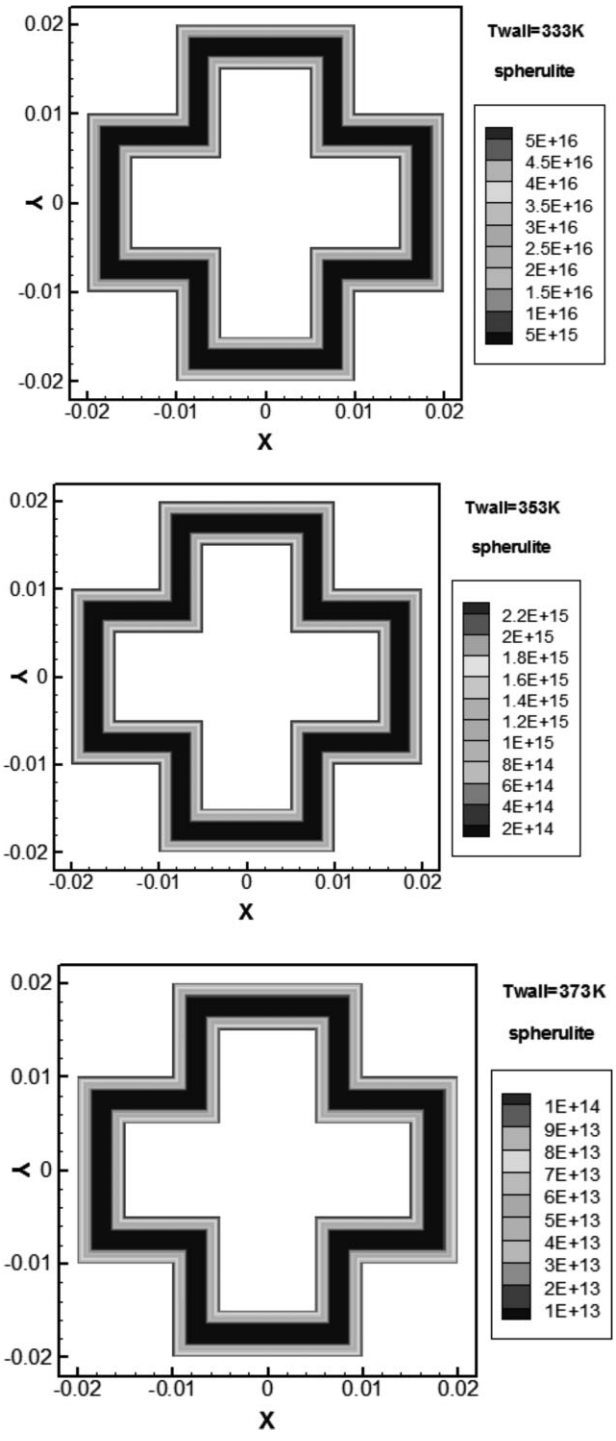

Figure 12. Variation of the nucleation density of spherulite with different thermal state on the $z = 0.02$ cross-section at $t = 5$ s ($Q_v = 1.4 \times 10^{-5}\ m^3 \cdot s^{-1}$).

lization kinetics process. Figure 12 and 13, respectively, show the variation of the nucleation density and average crystallite radius of the thermally induced spherulite with different thermal state on the $z = 0.02$ cross-section at $t = 5$ s ($Q_v = 1.4 \times 10^{-5}\ m^3 \cdot s^{-1}$). It can be found that the nucleation density increases with the decrease of temperature on the die wall. And meanwhile, the average crystallite radius of spherulite is found to be extended for the

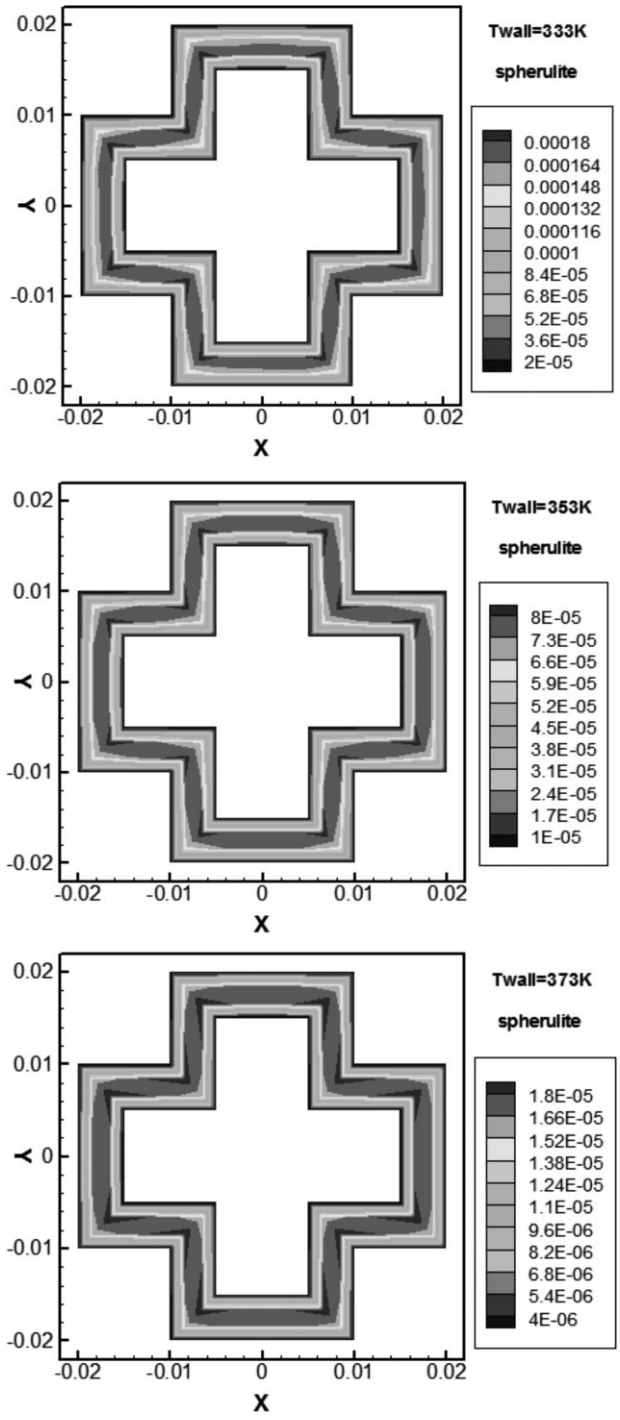

Figure 13. Variation of the average crystallite radius of spherulite with different thermal state on the $z = 0.02$ cross-section at $t = 5$ s ($Q_v = 1.4 \times 10^{-5}$ m$^3 \cdot$ s^{-1}).

increase of supercooling degree under the condition of lower die wall temperature. So in practical polymer processing, lower die wall temperature can on one hand accelerate the crystallization kinetics process, while on the other hand result in rough crystalline structure and the physical properties of final products like strength and toughness can be reduced.

5. Conclusion

The three-dimensional thermally and flow induced crystallization behavior of polymer melts in the hollow profile extrusion process has been simulated by using penalty finite element-finite difference method with a decoupled solving algorithm. The coexistence model of spherulite and shish-kebab was proposed to describe the evolution of crystallization kinetics process by using two sets of Schneider equation and Eder equation. The theoretical model and numerical method proposed in the study can not only describe the variation of macroscopic rheological parameters but also provide information on the variation of crystallizing morphology. With the standard Galerkin formulation adopted as basic computational framework, the discrete elastic viscous stress splitting algorithm in cooperating with the streamline upwinding approach can serve as a relatively robust numerical scheme. Due to the modest demand on computational memory, the method can be used to solve large-scale problems on small-scale computer systems. The proposed mathematical model and numerical solving method have been successfully applied to the investigation of crystallization behavior of polymer melts in the hollow profile extrusion process. It was found that both the flow and thermomechanical history can significantly influence the crystallization kinetics process when polymer melts extruded from the extrusion die to the cooling shaped mould, and hence affect the inner structure and physical property of final products. It is a preliminary application of the coexistence model of spherulite and shish-kebab for the investigation of crystallization behavior in polymer processing. Further considerations on how to improve inner structure and property of final products through proper control of processing conditions that are of significant interest for practical engineering problems will be introduced in the future work.

Nomenclature

$\boldsymbol{u}$	velocity vector
p	hydrostatic pressure
$\boldsymbol{\tau}$	extra stress tensor
$\boldsymbol{d}$	deformation rate tensor
$\boldsymbol{S}$	polymer-contribution stress
η_v	Newtonian-contribution viscosity
η_p	polymer-contribution viscosity
λ	relaxation time
$\overline{\eta}$	reference viscosity
ε	elasticity parameter

ξ	slip parameter
λ_p	penalty factor
ρ	material density
C_p	specific heat
k	thermal conductivity
α_∞	absolute crystallinity
α	relative crystallinity
ΔH_c	latent heat of crystallization
T_m	equilibrium melting temperature
U^*	activation energy
R	gas constant
T_g	glass transition temperature

Acknowledgements: This work is financially supported by the Natural Science Foundation of China (no. 51205231), the China Postdoctoral Science Foundation Special Funded Project (no. 201104621), the Program for Changjiang Scholars and Innovative Research Team in University of Ministry of Education of China (no. IRT0931) and the Natural Science Foundation of Shandong Province (no. ZR2012EEQ001).

Received: April 25, 2012; Revised: July 31, 2012; Published online: November 20, 2012; DOI: 10.1002/mats.201200028

Keywords: crystallization; modeling; shish-kebab; simulation; spherulite

[1] A. K. Doufas, *J. Rheol.* **2006**, *50*, 749.
[2] S. Acierno, S. Coppola, N. Grizzuti, *J. Rheol.* **2008**, *52*, 551.
[3] R. I. Tanner, F. Qi, *J. Non-Newtonian Fluid Mech.* **2005**, *127*, 131.
[4] H. Zuidema, G. W. M. Peters, H. E. H. Meijer, *Macromol. Theory Simul.* **2001**, *10*, 447.
[5] R. Zheng, P. K. Kennedy, *J. Rheol.* **2004**, *48*, 823.
[6] M. Stadlbauer, H. Janeschitz-Kriegl, G. Eder, E. Ratajski, *J. Rheol.* **2004**, *48*, 631.
[7] F. Y. Yu, H. B. Zhang, H. Zheng, W. Yu, C. X. Zhou, *Eur. Polym. J.* **2008**, *44*, 79.
[8] N. Phan-Thien, R. I. Tanner, *J. Non-Newtonian Fluid Mech.* **1977**, *2*, 353.
[9] W. Schneider, A. Koppl, J. Berger, *Int. Polym. Process.* **1988**, *2*, 151.
[10] M. Zinet, R. E. Otmani, M. Boutaous, P. Chantrenne, *Polym. Eng. Sci.* **2010**, *50*, 2044.
[11] J. V. Meerveld, M. Hütter, G. W. M. Peters, *J. Non-Newtonian Fluid Mech.* **2008**, *150*, 177.
[12] H. Zuidema, "Flow Induced Crystallization of Polymers," *PhD Thesis*, Eindhoven University of Technology, 2000.
[13] Y. Mu, G. Q. Zhao, H. P. Li, *Polym. Int.* **2009**, *58*, 475.
[14] R. Guenette, M. Fortin, *J. Non-Newtonian Fluid Mech.* **1995**, *60*, 27.
[15] J. M. Marchal, M. J. Crochet, *J. Non-Newtonian Fluid Mech.* **1987**, *26*, 77.
[16] A. N. Brooks, T. J. R. Hughes, *Comput. Methods Appl. Mech. Eng.* **1982**, *32*, 199.
[17] E. Koscher, R. Fulchiron, *Polymer* **2002**, *43*, 6931.